The first observation of azo-hydrazone and cis-trans tautomerisms for Disperse Yellow dyes and their nickel(II) and copper(II) complexes

Wei You, Hao-Yu Zhu, Wei Huang, Bin Hu, Ying Fan and Xiao-Zeng You

Electronic Supporting Information

Materials and measurements. Disperse Yellow dyes cis/trans-H$\mathbf{L_1}$ and cis-H$\mathbf{L_2}$ are prepared by referring a literature method. All other solvents and reagents were of analytical grade and used without further purification. Elemental analyses (EA) were measured with a Perkin-Elmer 1400C analyser. Infrared spectra (4000~400 cm^{-1}) were recorded on a Nicolet FTIR 170X spectrophotometer. ^1H NMR spectra were obtained in a Bruker 500 MHz NMR spectrometer. UV/visible (UV/Vis) spectra were recorded with a Shimadzu UV-3100 double-beam spectrophotometer using a Pyrex cell with a path length of 10 mm at room temperature. Powder X-ray diffraction (XRD) measurements were performed on a Philips X′pert MPD Pro X-ray diffractometer using Cu $K\alpha$ radiation (λ = 0.15418 nm), in which the X-ray tube was operated at 40 kV and 40 mA at room temperature. Thermogravimetric and differential thermal analyses (TG-DTA) were carried out by a NETZSCH STA449C instrument in argon flow from 30 to 800□ at a rate of 10.0□·min^{-1}.

X-ray data collection and solution. Single-crystal samples of cis/trans-H$\mathbf{L_1}$, cis-H$\mathbf{L_2}$ and dye-metal complexes **3**~**5** were glue-covered and mounted on glass fibers and used for data collection at 291(2) K on a Bruker SMART 1K CCD diffractometer using graphite mono-chromated MoKα radiation (λ = 0.71073 Å).[1] The crystal systems were determined by Laue symmetry and the space groups were assigned on the basis of systematic absences using XPREP, and then the structures were solved by direct method and refined by least-squares method on F_{obs}^2 by using the SHELXTL-PC software package.[2-3] All non-hydrogen atoms were refined on F^2 by full-matrix least-squares procedure using anisotropic displacement parameters.

Hydrogen atoms were inserted in the calculated positions assigned fixed isotropic thermal parameters at 1.2 times the equivalent isotropic U of the atoms to which they are attached (1.5 times for the methyl groups and oxygen atoms) and allowed to ride on their respective parent atoms. In complex **5**, the methyl unit (C7) of *N*-substituted ethyl group and one chlorine atom (Cl1) of phenyl ring in ligand $\mathbf{L_3}$ are refined over two sites in 0.676(12):0.324(12) and 0.731(4):0.269(4) site occupancy factors. The summary of the crystal data, experimental details and refinement results for cis/trans-H$\mathbf{L_1}$, cis-H$\mathbf{L_2}$ and metal complexes **3**~**5** is listed in Table ESI1, while selected bond distances and bond angles are given in Table ESI2. Hydrogen bonding interactions in cis/trans-H$\mathbf{L_1}$, cis-H$\mathbf{L_2}$, complexes **3** and **5** in are shown in Table ESI3.

Quantum chemical calculations for different conformational isomers of $\mathbf{HL_1}$ and $\mathbf{HL_2}$ dyes. On considering that the subtle change of substituted groups of the dye backbone (ethyl group in H$\mathbf{L_1}$ *versus* methyl group in H$\mathbf{L_2}$) can result in the cis/trans conformational alteration and possible azo-hydrazone tautomerism for the two Disperse Yellow dyes, we have carried out some computational studies for different isomers in cis/trans-H$\mathbf{L_1}$ and cis-H$\mathbf{L_2}$ molecules.

All the Density Function Theory computations are performed with the Gaussian 03, Revision C.02 programs[4] using the MPW1PW91 method and the LanL2DZ basis set. The fixed atom coordinates of cis-H$\mathbf{L_1}$, trans-H$\mathbf{L_1}$ and cis-H$\mathbf{L_2}$, originating from the structural parameters determined by the X-ray diffraction method, are used as the input files for the total energy calculations.

We have concluded in one of our papers that both of the experimental and theoretical studies demonstrate the existence in the hydrazone form for this family of azo dyes in the solid state which can be further stabilized by single or multiple six-membered intramolecular hydrogen-bonded rings.[13] In this work, both of Disperse Yellow dyes H$\mathbf{L_1}$ and H$\mathbf{L_2}$ adopt the same hydrazone form and six-membered intramolecular hydrogen-bonded rings are formed in their solid-state structures, which are well consistent with our previous conclusions. After we have calculated the energy differences between the energy-minimized pyridine-2,6-dione and

2-hydroxy-6-pyridone isomers of cis-H**L**$_1$, trans-H**L**$_1$, cis-H**L**$_2$ and trans-H**L**$_2$, it is found that all the pyridine-2,6-dione isomers are somewhat more thermally stable than the 2-hydroxy-6-pyridone isomers (Table ESI4), predominating the formation of hydrazone form. The energy gaps between the two tautomeric isomers are 150.40, 150.67, 148.64 and 149.63 KJ/mol, respectively, which are comparable with those of our previously reported C.I. Disperse Yellow dyes 114, 119, 126 and 211 (153.5 ~ 168.1 KJ/mol).

Besides the common azo and hydrazone isomeric forms, Disperse Yellow dyes H**L**$_1$ and H**L**$_2$ have cis and trans isomers originating from the presence of two chlorine atoms bonded to the phenyl ring, which is different from all the previously reported structures. In Table 3, we also summarize the computational details of the cis and trans isomers of H**L**$_1$ and H**L**$_2$ dyes. The energy gaps between the single-crystal structures and the energy-minimized structures in the same hydrazone form for the cis and trans isomers of H**L**$_1$ and the cis isomer of H**L**$_2$ are 603.69, 590.07 and 523.02 KJ/mol, respectively. The energy gap between the single-crystal structures of cis and trans isomers of H**L**$_1$ is 14.68 KJ/mol, while that between the energy-minimized structures of cis and trans isomers of H**L**$_1$ is only 1.06 KJ/mol. In contrast, the energy gap between the energy-minimized structures of cis and trans isomers of H**L**$_2$ is only 0.99 KJ/mol.

The results indicate that the trans isomers are a little more thermally stable than the cis ones for both of H**L**$_1$ and H**L**$_2$ molecules. Moreover, both isomers are accessible isomers because the energy gaps fall within the range of typical interactions in supramolecular level (several to tens of KJ/mol). The larger energy gaps between the single-crystal structures and the energy-minimized structures in the same hydrazone form for the cis and trans isomers of H**L**$_1$ and the cis isomer of H**L**$_2$ may be the reflection of the energy compensation of the formation of multiple hydrogen bonding and π–π stacking interactions between neighboring molecules.

References

(1) SMART and SAINT. Area Detector Control and Integration Software; Madison, Wisconsin (USA): Siemens Analytical X-Ray Systems, Inc.; **2000**.

(2) G. M. Sheldrick SADABS, Program for Empirical Absorption Correction of Area Dectector Data, Univ. of Gottingen, Germany; 2001.

(3) G. M. Sheldrick, SHELXTL (*Version 6.10*) Software Reference Manual; Madison, Wisconsin (USA): Bruker AXS, Inc.; 2000.

(4) M. J. Frisch, G. W. Trucks, H. B. Schlegel, G. E. Scuseria, M. A. Robb, J. R. Cheeseman, J. A. Montgomery, Jr., T. Vreven, K. N. Kudin, J. C. Burant, J. M. Millam, S. S. Iyengar, J. Tomasi, V. Barone, B. Mennucci, M. Cossi, G. Scalmani, N. Rega, G. A. Petersson, H. Nakatsuji, M. Hada, M. Ehara, K. Toyota, R. Fukuda, J. Hasegawa, M. Ishida, T. Nakajima, Y. Honda, O. Kitao, H. Nakai, M. Klene, X. Li, J. E. Knox, H. P. Hratchian, J. B. Cross, C. Adamo, J. Jaramillo, R. Gomperts, R. E. Stratmann, O. Yazyev, A. J. Austin, R. Cammi, C. Pomelli, J. W. Ochterski, P. Y. Ayala, K. Morokuma, G. A. Voth, P. Salvador, J. J. Dannenberg, V. G. Zakrzewski, S. Dapprich, A. D. Daniels, M. C. Strain, O. Farkas, D. K. Malick, A. D. Rabuck, K. Raghavachari, J. B. Foresman, J. V. Ortiz, Q. Cui, A. G. Baboul, S. Clifford, J. Cioslowski, B. B. Stefanov, G. Liu, A. Liashenko, P. Piskorz, I. Komaromi, R. L. Martin, D. J. Fox, T. Keith, M. A. Al-Laham, C. Y. Peng, A. Nanayakkara, M. Challacombe, P. M. W. Gill, B. Johnson, W. Chen, M. W. Wong, C. Gonzalez, J. A. Pople, *Gaussian 03, Revision C.02*; Gaussian, Inc.: Pittsburgh, PA, 2004.

Table ESI1. Computational details for four Disperse Yellow dye isomers (the total energy in KJ/mol and the dipole moment in C·m)

Compounds	*cis*-H$\mathbf{L_1}$	*trans*-H$\mathbf{L_1}$	*cis*-H$\mathbf{L_2}$	*trans*-H$\mathbf{L_2}$
Calculation methods / Basis set	DFT / MPW1PW91 / LanL2DZ			
Energy / Dipole moment (derived from the single-crystal structures in the hydrazone form)	-2564114.32 / 1.68×10^{-29}	-2564129.00 / 2.12×10^{-29}	-2461105.16 / 1.61×10^{-29}	-
Energy / Dipole moment (derived from the energy-minimized structures in the hydrazone form)	-2564718.01 / 1.43×10^{-29}	-2564719.07 / 2.13×10^{-29}	-2461628.18 / 1.48×10^{-29}	-2461629.17 / 2.13×10^{-29}
Energy / Dipole moment (derived from the energy-minimized structures in the azo form)	-2564567.61 / 1.74×10^{-29}	-2564568.40 / 2.87×10^{-29}	-2461479.54 / 1.67×10^{-29}	-2461479.54 / 2.85×10^{-29}

Table ESI2. Selected bond distances (Å) and metal containing bond angles (º) for cis/trans-H$\mathbf{L_1}$, cis-H$\mathbf{L_2}$ and metal complexes **3**~**5**

cis/trans-H$\mathbf{L_1}$				cis-H$\mathbf{L_2}$	
Bond distances					
C1–N3	1.316(6)	C16–N7	1.340(6)	C1–N3	1.320(5)
C1–C5	1.438(6)	C16–C20	1.433(7)	C1–C5	1.438(6)
C1–C2	1.470(7)	C16–C17	1.438(7)	C1–C2	1.463(6)
C2–O1	1.233(5)	C17–O3	1.233(6)	C2–O1	1.233(5)
C2–N1	1.381(6)	C17–N5	1.392(6)	C2–N1	1.376(5)
C3–O2	1.223(5)	C18–O4	1.214(6)	C3–O2	1.223(5)
C3–C4	1.458(7)	C18–N5	1.400(7)	C3–N1	1.383(5)
C3–N1	1.386(6)	C18–C19	1.475(7)	C3–C4	1.467(6)
N3–N4	1.318(5)	N7–N8	1.298(5)	N3–N4	1.294(4)
C8–N2	1.140(6)	C23–N6	1.130(7)	C7–N2	1.146(6)
3		**4**		**5**	
Bond distances					
Ni1–O1	1.975(6)	Cu1–O1	1.956(5)	Cu1–O1	1.934(5)
Ni1–N4	2.071(9)	Cu1–N4	1.975(6)	Cu1–O3	1.959(5)
Ni1–O3	2.116(9)	Cu1–N2^{b}	2.519(7)	Cu1–O4	2.273(5)
O1–C2	1.218(11)	C1–N3	1.354(10)	Cu1–N4	1.919(6)
O2–C3	1.217(14)	C1–C5	1.437(10)	Cu1–N2^{d}	1.961(7)
O3–C16	1.340(16)	C1–C2	1.446(12)	C1–N3	1.358(9)
N1–C2	1.408(13)	C2–O1	1.265(8)	C1–C5	1.394(9)
N1–C3	1.411(13)	C2–N1	1.389(10)	C1–C2	1.452(9)
N1–C6	1.437(17)	C3–O2	1.186(10)	C2–O1	1.243(8)
N3–N4	1.276(12)	C3–N1	1.413(10)	C2–N1	1.373(9)
N3–C1	1.373(14)	C3–C4	1.460(12)	C3–O2	1.223(8)
N4–C10	1.380(15)	C4–C5	1.384(11)	C4–C5	1.370(9)
C1–C2	1.412(15)	C4–C8	1.443(10)	C4–C8	1.448(11)
C1–C5	1.459(14)	N3–N4	1.291(8)	N3–N4	1.268(7)
N2–C8	1.107(16)	C8–N2	1.140(9)	C8–N2	1.138(9)
Bond angles					
O1–Ni1–N4	87.0(3)	O1–Cu1–N4	87.6(3)	O1–Cu1–O3	168.2(2)
O1–Ni1–O1^{a}	171.4(6)	O1–Cu1–O1^{b}	180.0(3)	O1–Cu1–O4	94.6(2)
O1–Ni1–N4^{a}	98.6(4)	O1–Cu1–N4^{b}	92.4(3)	N4–Cu1–O1	89.9(2)
O1–Ni1–O3	89.0(4)	O1–Cu1–N2^{b}	90.3(2)	N4–Cu1–O3	84.7(3)
O1–Ni1–O3^{a}	84.6(3)	O1–Cu1–N2^{c}	89.7(2)	N4–Cu1–N2^{d}	168.8(3)
N4–Ni1–O3	88.3(4)	N4–Cu1–N2^{b}	95.2(3)	O1–Cu1–N2^{d}	89.9(3)
N4–Ni1–O3^{a}	169.1(4)	N4–Cu1–N2^{c}	84.8(3)	O3–Cu1–N2^{d}	93.3(3)
N4–Ni1–N4^{a}	99.9(6)	N4–Cu1–N4^{b}	180.000(1)	N4–Cu1–O4	93.7(2)
O3–Ni1–O3^{a}	84.6(6)	N2^{b}–Cu1–N2^{c}	180.0(0)	O3–Cu1–O4	96.3(2)

Symmetry codes: ^{a}, 3/2-*x*, 3/2-*y*, z; ^{b}, 1-*x*, 1-*y*, 1-*z*; ^{c}, -1+*x*, 1+*y*, *z*; ^{d}, -1/2+*x*, 3/2-*y*, 1/2+*z*.

Table ESI3. Hydrogen bonding interactions (Å, °) in cis/trans-H$\mathbf{L_1}$, cis-H$\mathbf{L_2}$ and metal complexes **3**~**5**

D–H…A	D–H	H…A	D…A	∠DHA	Symmetry code
cis/trans-H$\mathbf{L_1}$					
N4–H4…O1	0.86	1.90	2.576(6)	134.0	
N8–H8…O3	0.86	1.97	2.623(6)	132.0	
C14–H14…N6	0.93	2.55	3.244(9)	132.0	-*x*, 1-*y*, 1-*z*
C15–H15…O4	0.93	2.53	3.433(7)	163.0	-*x*, 1-*y*, 1-*z*
C24–H24B…O2	0.96	2.59	3.469(7)	153.0	1-*x*, -1/2+*y*, 3/2-*z*
C26–H26…O2	0.93	2.36	3.216(7)	154.0	*x*, 1/2-*y*, -1/2+*z*
cis-H$\mathbf{L_2}$					
N4–H4…O1	0.86	1.90	2.576(4)	134.0	
C8–H8A…N2	0.96	2.61	3.500(7)	154.0	1-*x*, 2-*y*, 2-*z*
3					
O3–H3A…N2	0.85	2.05	2.823(15)	151.0	2-*x*, *y*, -1/2+*z*
C14–H14…O2	0.93	2.38	3.191(16)	145.0	-1/2+*x*, 3/2-*y*, 1/2+*z*
C15–H15…N4	0.93	2.58	3.382(15)	145.0	3/2-*x*, 3/2-*y*, *z*
5					
O4–H4A…N2	0.85	2.59	3.329(9)	146.0	1/2-*x*, 1/2+*y*, 3/2-*z*
O4–H4A…O3	0.85	2.14	2.847(7)	140.0	-*x*, 2-*y*, 2-*z*
O4–H4B…Cl1	0.85	2.70	3.410(6)	143.0	-*x*, 2-*y*, 2-*z*

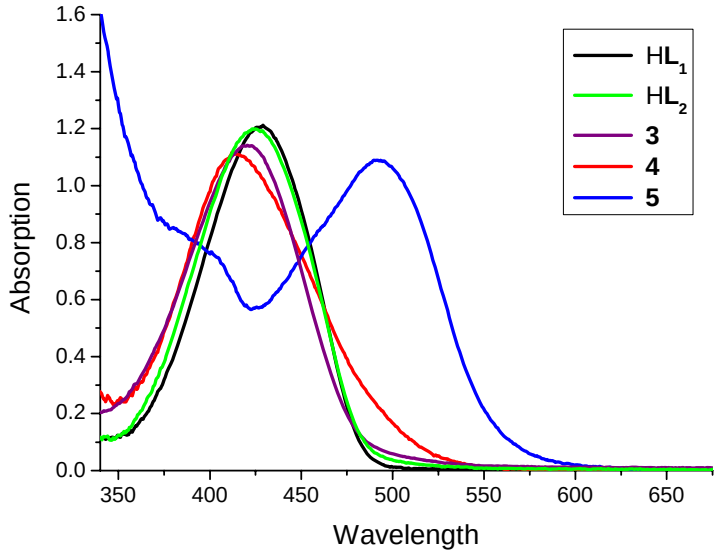

Fig. ESI1. UV/Vis spectra of five compounds in methanol solutions.

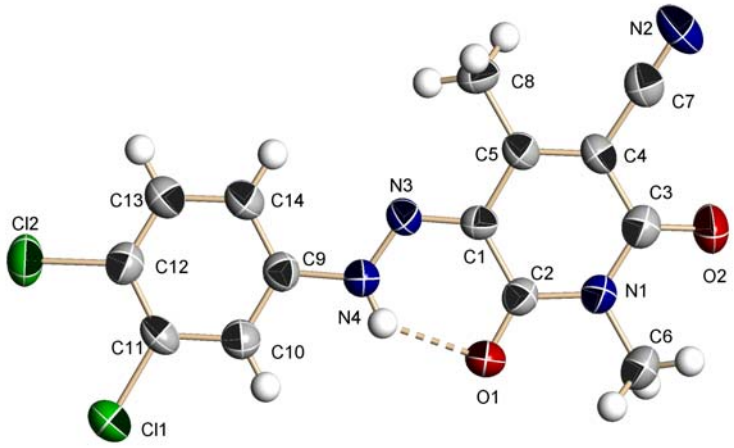

Fig. ESI2. ORTEP drawing of Disperse Yellow dye cis-H**L**$_2$ with the atom-numbering scheme. Displacement ellipsoids are drawn at the 30% probability level and the H atoms are shown as small spheres of arbitrary radii.

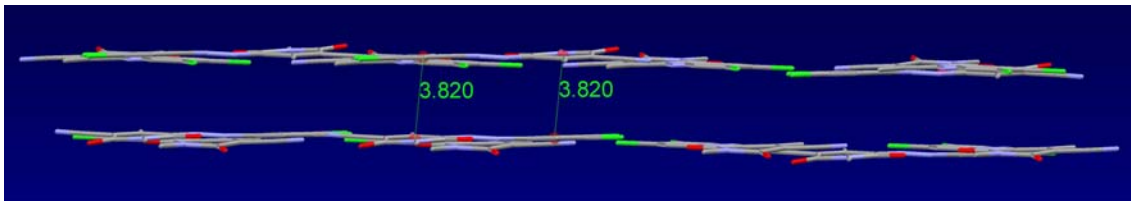

Fig. ESI3. Perspective view of the layer packing structure of cis-H**L**$_2$ showing the centroid-centroid separation (Å) between π-π stacking aromatic rings.

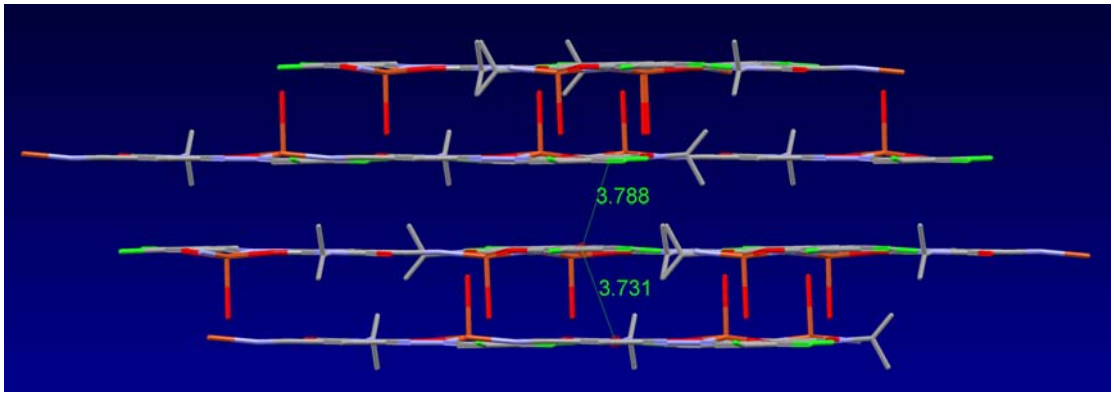

Fig. ESI4. Packing diagram of **5** showing the centroid-centroid separations (Å) for π-π stacking between and within different dimeric units.

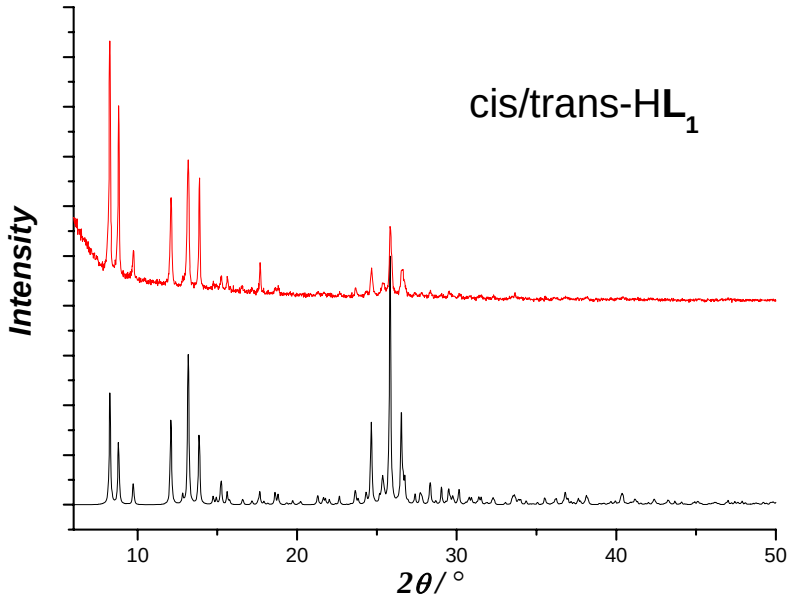

Fig. ESI5. The simulative (black line) and experimental (red line) powder X-ray diffraction patterns for compound cis/trans-H$\mathbf{L_1}$.

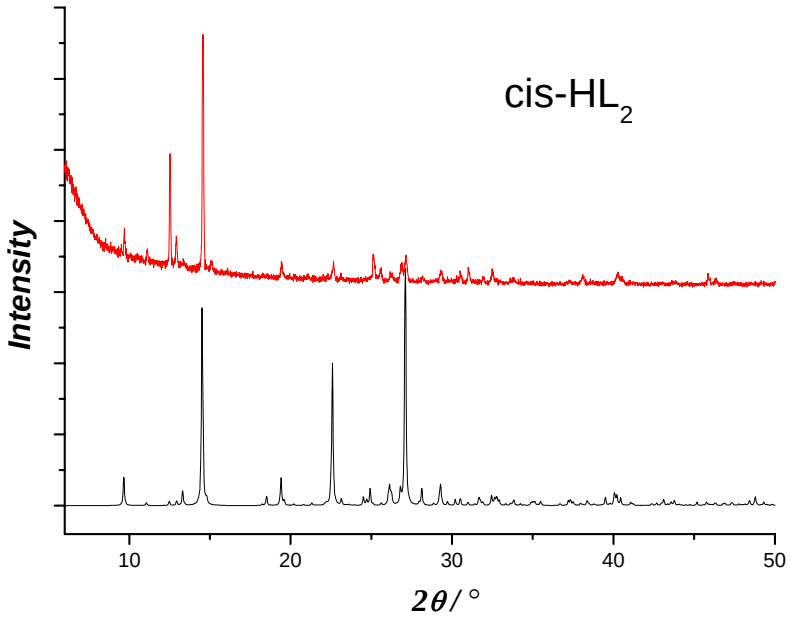

Fig. ESI6. The simulative (black line) and experimental (red line) powder X-ray diffraction patterns for compound cis-H**L$_2$**.

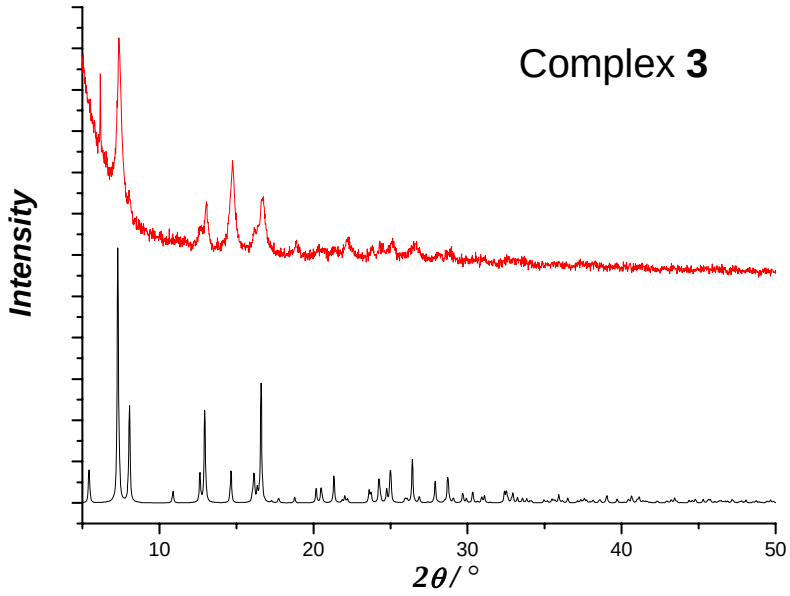

Fig. ESI7. The simulative (black line) and experimental (red line) powder X-ray diffraction patterns for complex **3**.

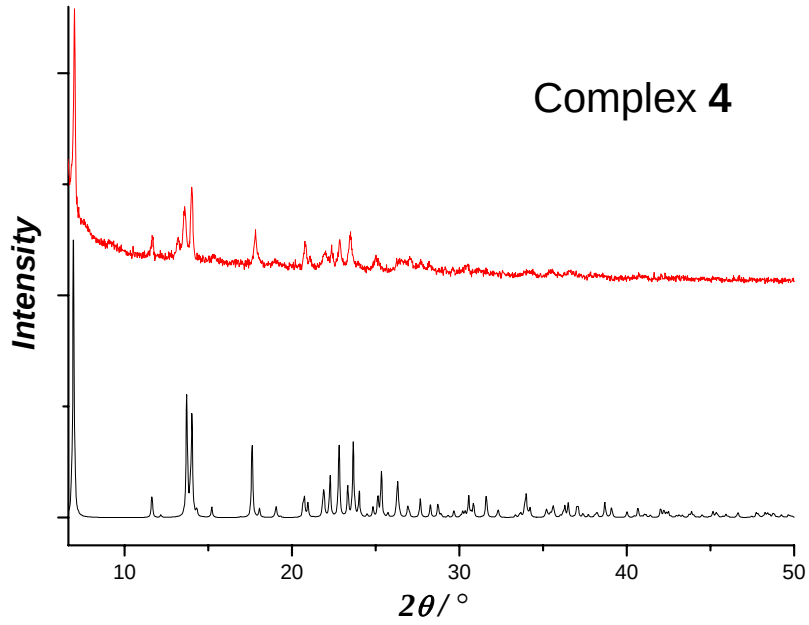

Fig. ESI8. The simulative (black line) and experimental (red line) powder X-ray diffraction patterns for complex **4**.

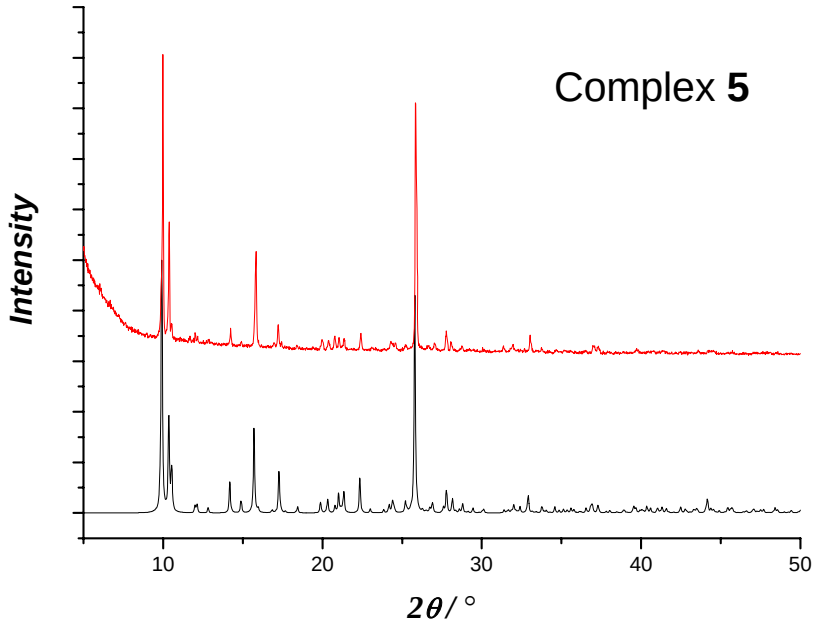

Fig. ESI9. The simulative (black line) and experimental (red line) powder X-ray diffraction patterns for complex **5**.

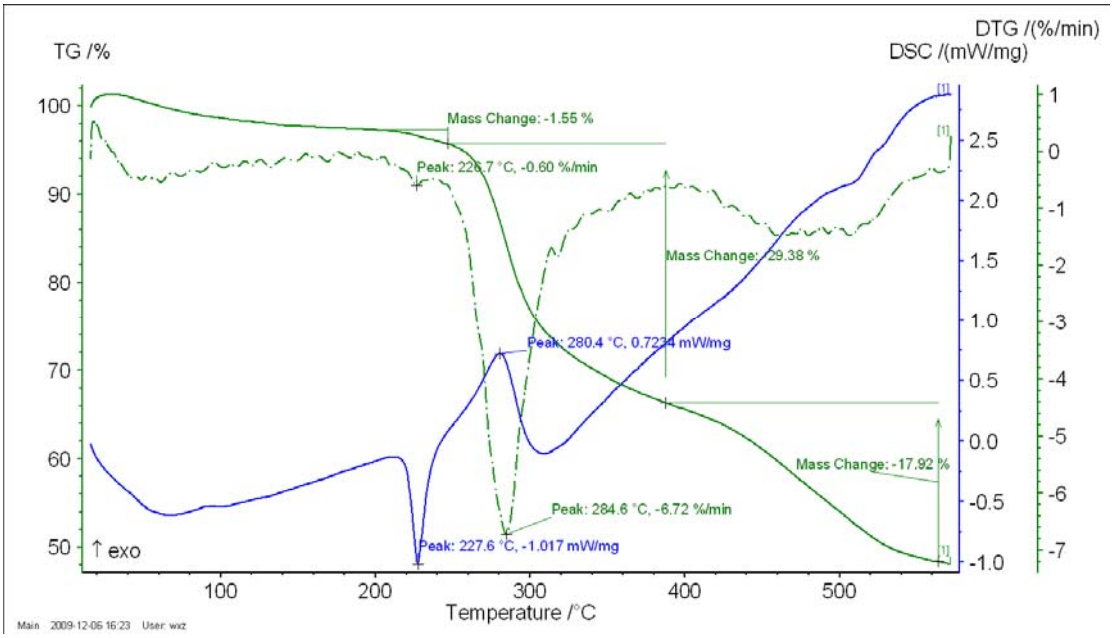

Fig. ESI10. Diagram of TG-DTA analyses for compound cis/trans-H$\mathbf{L_1}$.

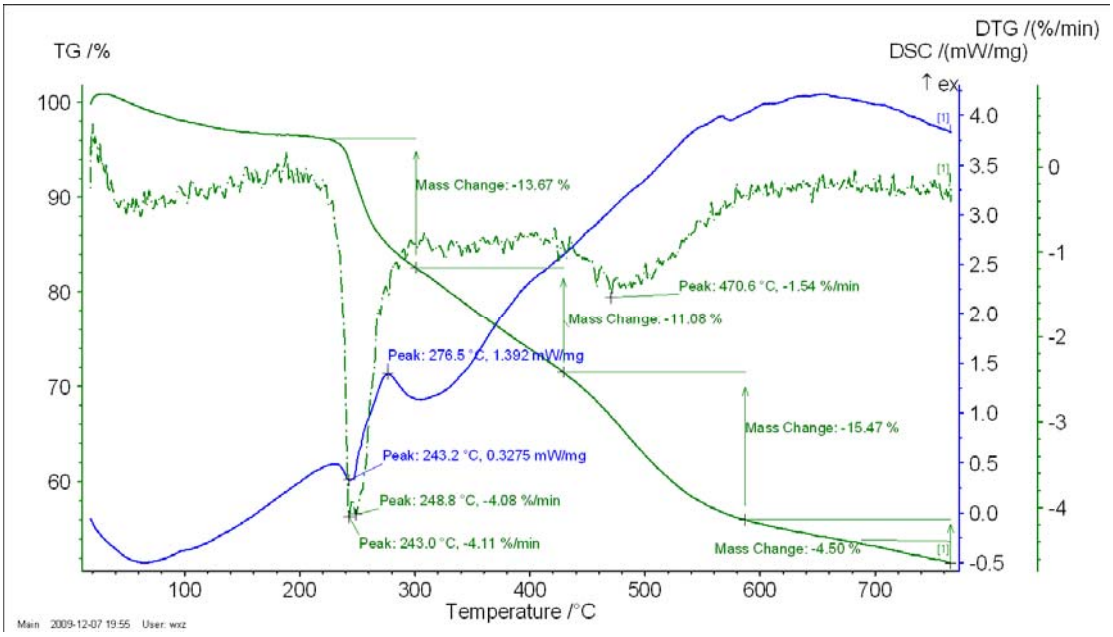

Fig. ESI11. Diagram of TG-DTA analyses for compound cis-H$\mathbf{L_2}$.

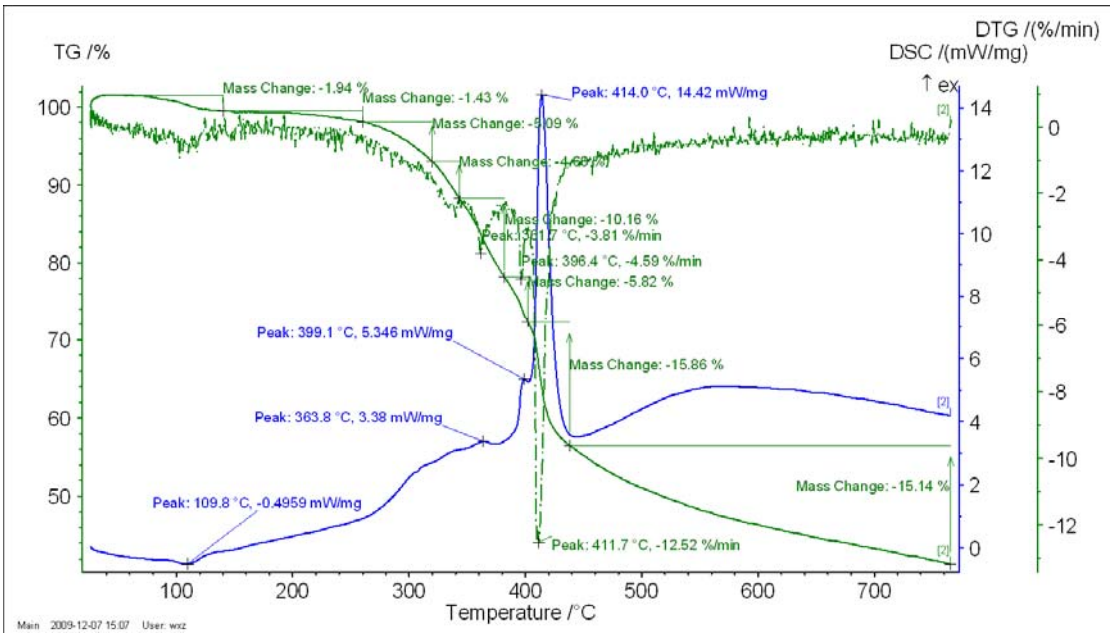

Fig. ESI12. Diagram of TG-DTA analyses for complex **3**.

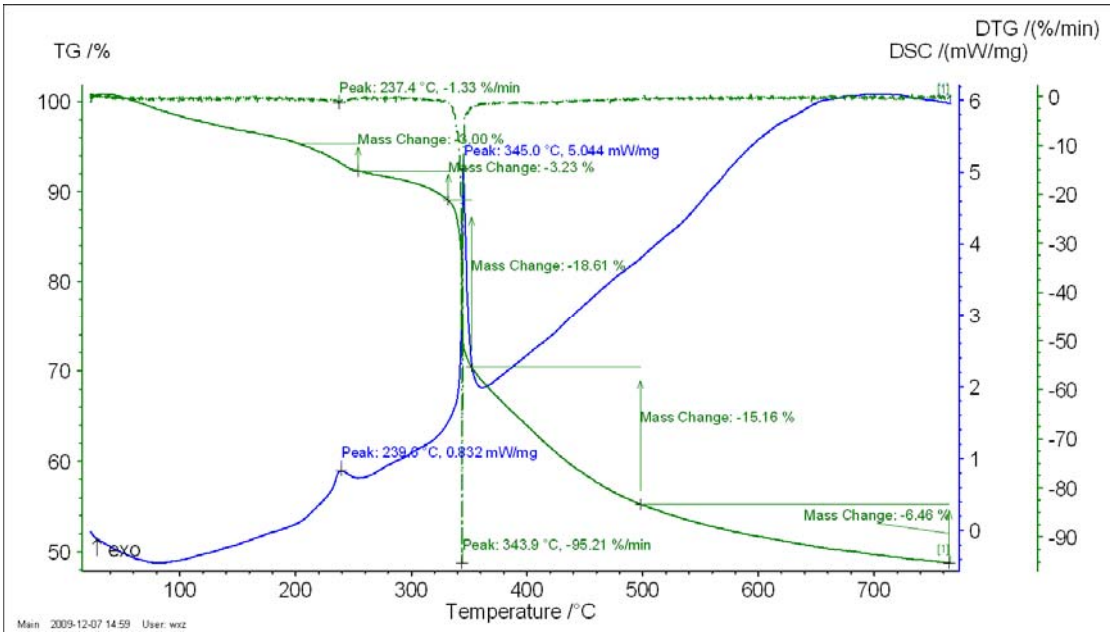

Fig. ESI13. Diagram of TG-DTA analyses for complex **4**.

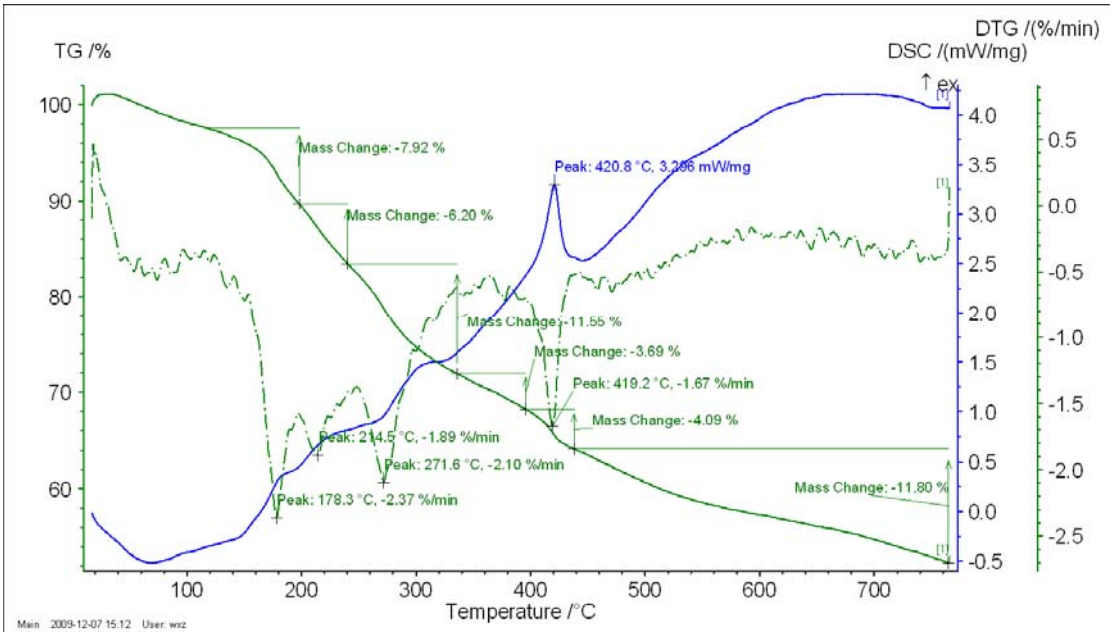

Fig. ESI14. Diagram of TG-DTA analyses for complex **5**.